25. H.-Y. Tsai, H. I. Smith, R. Menon, *Opt. Lett.* **33**, 2916 (2008).
26. S. W. Hell, *Nat. Biotechnol.* **21**, 1347 (2003).
27. We thank F. Stellacci and T. Swager for advice on synthesis of the photochromic molecules, H. Koh for the ellipsometric measurements, T. O'Reilly for assistance with the Lloyd's-mirror interferometer, and H. Smith for suggestions on the manuscript. T.L.A. was partially funded by a subcontract (6916866) from LumArray. H.-Y.T. was partially funded by an ignition grant from the MIT Deshpande Center for Technological Innovation. R.M. was partially funded by a Defense Advanced Research Projects Agency Small Business Innovation Research award (W31P4Q-05-C-R156). Three patents have been filed through MIT based on the work presented herein.

Supporting Online Material
www.sciencemag.org/cgi/content/full/1167704/DC1
Materials and Methods
SOM Text
Figs. S1 to S6
Table S1
References

27 October 2008; accepted 24 February 2009
Published online 9 April 2009;
10.1126/science.1167704
Include this information when citing this paper.

Size and Shape of Saturn's Moon Titan

Howard A. Zebker,[1]* Bryan Stiles,[2] Scott Hensley,[2] Ralph Lorenz,[3] Randolph L. Kirk,[4] Jonathan Lunine[5]

Cassini observations show that Saturn's moon Titan is slightly oblate. A fourth-order spherical harmonic expansion yields north polar, south polar, and mean equatorial radii of 2574.32 ± 0.05 kilometers (km), 2574.36 ± 0.03 km, and 2574.91 ± 0.11 km, respectively; its mean radius is 2574.73 ± 0.09 km. Titan's shape approximates a hydrostatic, synchronously rotating triaxial ellipsoid but is best fit by such a body orbiting closer to Saturn than Titan presently does. Titan's lack of high relief implies that most—but not all—of the surface features observed with the Cassini imaging subsystem and synthetic aperture radar are uncorrelated with topography and elevation. Titan's depressed polar radii suggest that a constant geopotential hydrocarbon table could explain the confinement of the hydrocarbon lakes to high latitudes.

The Cassini spacecraft has been orbiting Saturn for 4 years, observing Titan periodically. When close to Titan, it can return surface elevation data from a nadir-pointing radar altimeter (*1*) and a multiple-beam synthetic aperture radar (SAR) imaging system (*2*, *3*). We have used these radar instrument modes to estimate the surface elevation by measuring the time delay of the altimeter echoes and the precise radar look angle to points on the surface by processing the multibeam SAR images with monopulse methods (Fig. 1) (*4*).

In the radar altimeter mode, the instrument transmits energy nearly vertically to the planetary surface below and records the received echo as a function of time; we corrected the data for biases due to mis-pointing errors (*1*). The Cassini altimetry data products record both the leading-edge location and the average delay of the return echo, but we used the mean return in order to estimate the mean surface height.

The SAR imaging system on Cassini comprises five parallel beams that produce a much wider ground swath than would have been possible with the use of a single beam. Each beam is time-shared in order to maintain a contiguous swath on the ground (*5*, *6*), so we sacrificed along-track resolution, averaging, and signal-to-noise ratio for the sake of the increased swath width. This is the burst-mode or ScanSAR imaging configuration, and it returns five overlapping observation swaths from the surface. The differencing of power images from the overlapped sections of adjacent beams forms an amplitude monopulse system to measure the precise angle to a given point on the ground (*4*, *7*), which, combined with knowledge of the spacecraft imaging geometry, yields a surface height measurement. Hence, under this analysis, most of the SAR imaging passes also provide estimates of the elevation at the beam overlap regions. Although this method is more elaborate than altimetry, it provides wider coverage because SAR imaging is used more often. We used all possible beam overlaps containing pixels sufficiently bright that the intensity differences were meaningful. The effective footprint of each measurement is roughly the SAR resolution (0.5 km) in the range direction and 10 km in the along-track direction.

These techniques show that the poles of Titan lie at lower elevations than the equator and that the topography also varies longitudinally (Fig. 1). Measurements in the polar regions yield elevations of about –600 to –700 m, referenced to a 2575-km-radius sphere, whereas Titan's

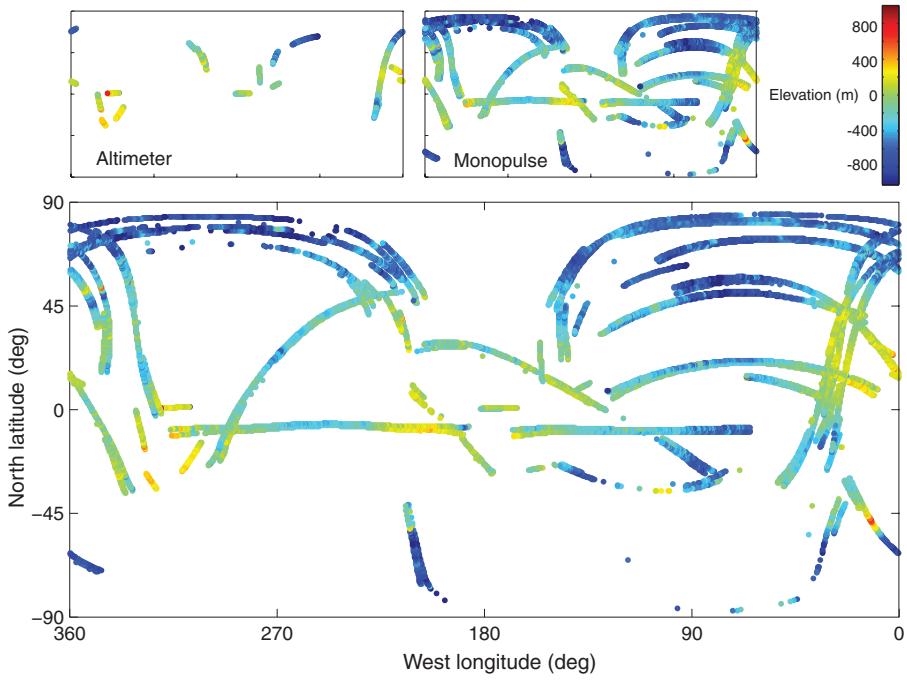

Fig. 1. Titan elevations observed with altimeter and SAR monopulse radar modes, cylindrical projection, displayed as deviation from an ideal 2575 km sphere located at Titan's barycenter. Locations on the figure give the latitude and west longitude of each measurement. Far more coverage is available from the monopulse mode than from altimetry, but these data are not as accurate as the altimeter measurements.

[1]Departments of Geophysics and Electrical Engineering, Stanford University, Stanford, CA 94305, USA. [2]Jet Propulsion Laboratory (JPL), California Institute of Technology, 4800 Oak Grove Drive, Pasadena, CA 91109, USA. [3]Applied Physics Laboratory, Johns Hopkins University, 11100 Johns Hopkins Road, Laurel, MD 20723, USA. [4]U.S. Geological Survey, 2255 North Gemini Drive, Flagstaff, AZ 86001, USA. [5]Departments of Planetary Science and Physics, University of Arizona, Tucson, AZ 85721, USA.

*To whom correspondence should be addressed. E-mail: zebker@stanford.edu

highest areas approach +400 m. Errors in both the altimetry and monopulse data depend mainly on ephemeris accuracy and spacecraft pointing control (*1*, *7*). The Cassini orbit reconstructions we used (*8*, *9*) are accurate at the 10- to several-hundred-meter level, with the out-of-plane component being most uncertain; pointing uncertainty leads to another 50 to 100 m for both data sets. Absolute errors up to 400 m are not uncommon on a point-by-point basis, because SAR monopulse measurements depend critically on pointing knowledge. We applied a network adjustment to reduce these raw errors by about a factor of 2 (*7*). We calculated formal errors in all of our solutions and found that for the low-order harmonic and ellipsoid solutions, errors ranged from 10 to 110 m (*10*), because we retrieved very few parameters in our inversion procedure, and we have 18 altimeter and 24 monopulse uncorrelated radar acquisition tracks. These uncertainties do not reflect systematic errors, such as any unknown degradation in the satellite ephemeris reconstruction on passes that diverge from the ecliptic plane, so that polar elevations may be systematically higher or lower because of errors in satellite position. A detailed description of the error analysis is given in the supporting online material (SOM).

Table 1. Best-fit surfaces to Titan elevation data. The ellipsoid axis *a* is the long axis pointing to Saturn, *c* is the polar axis, and *b* is the orthogonal equatorial axis. All results are in kilometers, except for rotations, which are in degrees.

	Ellipsoids			Spherical harmonics
	Sphere	Biaxial	Triaxial	Order 4
a axis	2574.97 ± 0.01	2575.06 ± 0.01	2575.15 ± 0.02	
b axis	2574.97 ± 0.01	2575.06 ± 0.01	2574.78 ± 0.06	
c axis	2574.97 ± 0.01	2574.51 ± 0.05	2574.47 ± 0.06	
a translation	0.03 ± 0.01	0.04 ± 0.02	0.06 ± 0.02	
b translation	0.30 ± 0.02	0.35 ± 0.02	0.39 ± 0.03	
c translation	−0.26 ± 0.02	−0.06 ± 0.03	−0.02 ± 0.03	
a axis rotation		−5.9° ± 2.6°	−16.2° ± 5.3°	
b axis rotation		0.9° ± 2.3°	4.6° ± 1.8°	
c axis rotation			0.9° ± 3.7°	
North polar radius	2574.71 ± 0.02	2574.46 ± 0.06	2574.47 ± 0.07	2574.32 ± 0.05
South polar radius	2575.23 ± 0.02	2574.58 ± 0.06	2574.52 ± 0.07	2574.36 ± 0.03
Mean equatorial radius	2574.97 ± 0.01	2575.05 ± 0.01	2574.95 ± 0.06	2574.91 ± 0.11
Mean radius				2574.73 ± 0.09
Data RMS misfit	0.32	0.28	0.26	0.19

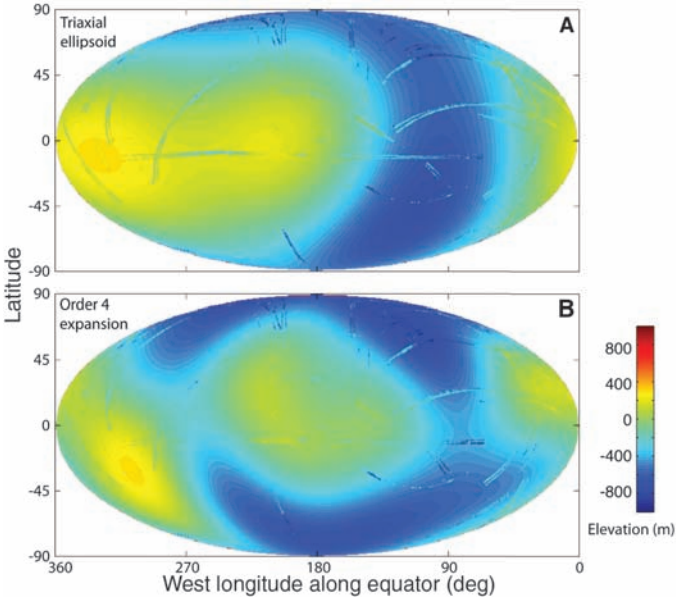

Fig. 2. (**A**) Best-fit translated, rotated, triaxial ellipsoid. Measurements are plotted on top of the ellipsoid, exhibiting contrast where they differ from the solution. Color indicates elevation relative to a 2575 km reference sphere at Titan's barycenter. Data plotted using a Mollweide projection to convey the areas associated with elevation features. (**B**) Fourth-order spherical harmonic fit to elevation data, using same conventions.

We used the data described above to estimate the global shape of Titan. We fit the observations to ellipsoids and to low-order spherical harmonic series to examine the global properties of the inferred shape. Both sets of solutions gave similar estimates for polar and equatorial radii but differed in the exact body shape we inferred. Because the data are relatively sparse, and particularly lacking in the far southern hemisphere, harmonic expansions tend to be highly oscillatory and error-prone for this region. Therefore, we used constrained inversion methods to discard the unlikely solutions that yet fit the data at the measured locations (*7*). We required the solution to be nearly spherical and selected the degree of constraint by examining the error in the data-sparse south polar region, picking its least value that still allowed matching this subset of observations. To find the reference sphere size, we iterated the solution until its mean radius was equal to the constraint radius.

We determined the best-fitting, translated, and rotated sphere, biaxial ellipsoid, and triaxial ellipsoid by minimizing the root mean square (RMS) difference between the observations and each solution, weighted by the uncertainty in the observations (Table 1) (*11*). The misfit of the solution ranges from 190 to 360 m RMS, showing that more degrees of freedom in the model lead to a better fit. The ellipsoid parameters follow from combinations of all data points and thus exhibit far less uncertainty than an individual elevation measurement. We used a diagonal approximation to the data covariance matrix, justifiable because the data collected on different passes are generally uncorrelated. For the ellipsoid solutions, the poles are of lower elevation than the equator; in the triaxial case, a local maximum occurs at about 330°W longitude (Fig. 2A).

The spherical harmonic fits also show that the poles are low and the equator is high (Fig. 2B). The details of the solutions are different but the general shape is maintained. In this fourth-

Table 2. Triaxial ellipsoid in synchronous rotation. The present value of q (ω^2R^3/GM) = 0.00003957. Calculated values are from first-order equations (*23*), with homogeneity parameter (H) = 1 for the homogeneous case and H = 0.56 for a layered Titan, assuming a mantle density of 0.9 g cm^{-3}.

	Observed	Calculated, homogeneous Titan		Calculated, layered Titan	
		q (at present)	$q' = q \times 1.25$	q (at present)	$q' = q \times 2.23$
Equatorial radius toward Saturn (*a*)	2575.15 ± 0.02	2575.10	2575.17	2574.97	2575.17
Orthogonal equatorial radius (*b*)	2574.78 ± 0.06	2574.72	2574.69	2574.75	2574.69
Polar radius (*c*)	2574.47 ± 0.06	2574.59	2574.53	2574.69	2574.53
RMS error (observed versus calculated)		0.08	0.06	0.16	0.06

order solution, a maximum occurs at 25°S, 305°W; other high-elevation regions can be found between ±45°N and 120° to 240°W. Spherical harmonics with other order expansions have a different elevation distribution but preserve the polar and mean equatorial values as seen above (Table 1; complete solutions up to the seventh order are given in the SOM).

The north and south polar radii are similar and agree within the formal errors for our solutions. The mean equatorial radius is very close to 2575 km. The ellipsoidal fits also show an offset between the center of figure and the center of mass, mainly in the along-orbit direction, of about 300 to 400 m. Although this could be a physical effect, it can also result from a nonellipsoidal Titan figure or even systematic spacecraft ephemeris errors.

We compared our measurements of Titan to those predicted from a uniform, synchronously rotating, triaxial spheroid model in hydrostatic equilibrium (Table 2). Our fit yields an equatorial bulge a-c of 0.68 km and an equatorial asymmetry a-b of 0.37 km, approximating the expected shape of an ellipsoid in synchronous rotation (*12*). The RMS misfit of the three observed ellipsoid radii to the theoretical homogeneous planet case is 0.08 km, and the fit can be made even closer (0.06 km) if we increase the ratio of centrifugal to gravitational acceleration at the satellite surface (q) (ω^2R^3/GM) (*12*) by 25% (ω, rotation rate; R, radius; G, gravitational constant; M, mass of Titan).

On the basis of thermal modeling (*13*, *14*) and measurements of changes in rotation rate, and by analogy with other large satellites, we expect Titan to have differentiated into a rock-rich, or possibly rock-iron, core with an outer ice/water mantle on the order of 100 km thick and crust that is less dense (~0.9 g cm^{-3}) than the global average density (1.88 g cm^{-3}). Under these conditions, q must be 2.23 times greater to minimize the misfit, implying that Titan's orbital radius was perhaps 77% of its present value when its shape was set. "Frozen-in" shapes from previous rotational states have been suggested for Earth, the Moon, Mars, and most recently for Iapetus (*15*). Although it may be unlikely that tidal dissipation in Saturn is responsible for any migration of Titan's orbit, other mechanisms are possible, analogous perhaps to the proposed expansion of giant-planet orbits around the Sun by planetesimal scattering (*16*). Titan's observed shape is more consistent with a body orbiting closer to Saturn.

Despite the closeness of fit of our observations to the triaxial ellipsoid just described, the ratio (b-c)/(a-c) for our data is 0.46 rather than the theoretical 0.25. Given our uncertainties, it is possible but not particularly likely that this ratio is 0.3 or even less, so that Titan may indeed be in hydrostatic equilibrium. Still, we cannot conclusively state that Titan is a synchronously rotating hydrostatic body.

Titan's geomorphology shows that substantial masses of surface material, in the form of polar lakes of liquid hydrocarbons or the equatorial dune sands, can be transported over global distance scales perhaps more quickly than the internal structure can adjust to changing loads (*17*, *18*). Although both dunes and lakes appear to be active today, we cannot say whether enough mass can be moved on time scales sufficiently short to lead to a shape inconsistent with Titan's present orbit. It is also possible, as has been proposed for Europa (*19*), that topography can result from uneven heating of the icy shell. If heating is greater at the poles than the equator, an apparent equatorial bulge is produced.

We plotted the fifth-order global elevation solution over an image mosaic derived from the Cassini imaging subsystem (*20*) in order to examine relationships between observed image features and elevation (Fig. 3). Xanadu (*21*) is the most prominent surface region and was long speculated to be elevated. The optical and radar images indicate that it is a very rough, mountainous terrain, but its regional elevation is low. Other large-scale surface features do not appear to be correlated with elevation in our solutions.

These global elevation solutions may help in understanding the distribution of the Titan lakes. The lakes occur mainly in the polar regions (*22*), with a preference for the north polar area in the data collected to date by Cassini. If we posit that the lakes are surface expressions of a more or less continuous liquid organic "water table," then the lower elevations of the poles could lead to the observed preponderance of lakes at high latitudes. However, whether the polar surface intersects a methane table depends on its distance from a constant gravity potential surface, and not on its elevation from the barycenter, because the equipotential may be depressed as well at the poles.

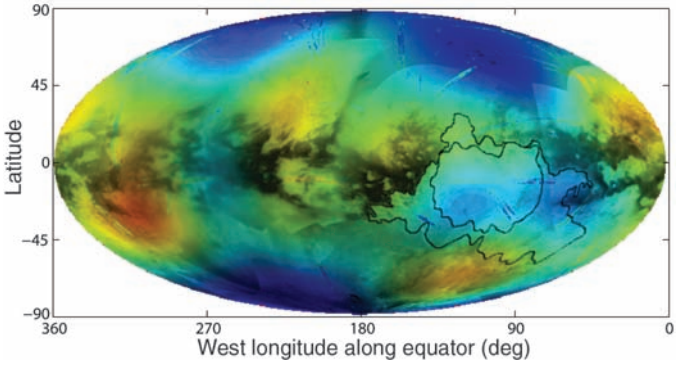

Fig. 3. Fifth-order solution (color) plotted over Cassini imaging mosaic of Titan surface. The outlined feature slightly south of the equator and west of 90° W is Xanadu, the largest identified region on Titan and believed to be a mountainous terrain. Two black outlines are shown. The inner region is the brightest portion of Xanadu, and the outer line denotes an extended Xanadu including less-dark but otherwise texturally similar material. Xanadu seems to be systematically lower than other parts of the equatorial belt, and not uplifted like most mountainous areas on Earth.

References and Notes

1. H. A. Zebker *et al.*, *Icarus* **200**, 240 (2009).
2. B. W. Stiles *et al.*, *Icarus*, 10.1016/j.icarus.2009.03.032 (2009).
3. C. Elachi *et al.*, *Science* **308**, 970 (2005).
4. D. R. Rhodes, *Introduction to Monopulse* (McGraw Hill, New York, 1959; reprinted by Artech House, Norwood, MA, 1980).
5. R. K. Moore, J. P. Claassen, Y. H. Lin, *IEEE Trans. Aero. Elec. Sys.* **AES-17**, 410 (1981).
6. C. Elachi *et al.*, *Proc. IEEE* **79**, 867 (1991).
7. See SOM on *Science* Online.
8. P. G. Antreasian *et al.*, American Astronomical Society (AAS) paper 2008-6747, presented at the American Institute of Aeronautics and Astronautics/AAS Astrodynamics Specialist Conference and Exhibit, Honolulu, HI, 18 to 21 August 2008.
9. The ephemeris we used was the JPL Cassini orbit solution as of October 2008.
10. The errors on each measurement are well known and range from tens of meters for the altimetry measurements to hundreds of meters for the SAR monopulse data (*1*, *8*, *9*) (SOM). The correlations in time for the spacecraft pointing and attitude knowledge errors, which dominate all of our observations, are less well known. We conservatively assumed that these errors are perfectly correlated along each pass (a constant attitude error) and uncorrelated between passes. We calculated formal errors using a diagonal approximation to the covariance matrix, subject to the assumption of correlated pointing errors for each acquisition.
11. The planetary radii given in Table 1 and elsewhere in the text are the distances from the specified location to the barycenter of Titan. The radii do not equal the corresponding ellipsoid axes if the best-fit ellipsoid is offset from the barycenter.
12. S. F. Dermott, *Icarus* **37**, 310 (1979).
13. A. D. Fortes *et al.*, *Icarus* **188**, 139 (2007).
14. G. Tobie, J. I. Lunine, C. Sotin, *Nature* **440**, 61 (2006).
15. J. C. Castillo-Rogez *et al.*, *Icarus* **190**, 179 (2007).
16. K. Tsiganis *et al.*, *Nature* **435**, 459 (2005).
17. G. Mitri *et al.*, *Icarus* **186**, 385 (2007).
18. J. W. Barnes *et al.*, *Icarus* **195**, 400 (2008).
19. G. W. Ojakangas, D. J. Stevenson, *Icarus* **81**, 220 (1989).
20. S. Albers, map of Titan derived from images at the Cassini Project Web site http://saturn.jpl.nasa.gov, available at http://laps.noaa.gov/albers/sos/sos.html.
21. C. C. Porco *et al.*, *Nature* **434**, 159 (2005).
22. E. R. Stofan *et al.*, *Nature* **445**, 61 (2007).
23. S. F. Dermott, *Icarus* **73**, 25 (1988).

24. We thank the Cassini Radar Team for detailed planning of these observations. This work was supported by the Cassini Project and by NASA as part of the Cassini Data Analysis Program. We also thank the reviewers for many constructive comments on our error analysis and data interpretation. The Cassini Project is a joint endeavor of NASA, the European Space Agency, and the Italian Space Agency. Cassini is managed by JPL, California Institute of Technology, under a contract with NASA.

Supporting Online Material

www.sciencemag.org/cgi/content/full/1168905/DC1
Materials and Methods
Figs. S1 to S4
Tables S1 to S3
References

24 November 2008; accepted 20 March 2009
Published online 2 April 2009;
10.1126/science.1168905
Include this information when citing this paper.